

Numerical study of ducted turbines in bi-directional tidal flows

M. Maduka & C.W. Li

To cite this article: M. Maduka & C.W. Li (2021) Numerical study of ducted turbines in bi-directional tidal flows, Engineering Applications of Computational Fluid Mechanics, 15:1, 194-209, DOI: [10.1080/19942060.2021.1872706](https://doi.org/10.1080/19942060.2021.1872706)

To link to this article: <https://doi.org/10.1080/19942060.2021.1872706>



© 2021 The Author(s). Published by Informa UK Limited, trading as Taylor & Francis Group.



Published online: 13 Jan 2021.



Submit your article to this journal [↗](#)



Article views: 879



View related articles [↗](#)



View Crossmark data [↗](#)

Numerical study of ducted turbines in bi-directional tidal flows

M. Maduka  and C.W. Li 

Department of Civil and Environmental Engineering, The Hong Kong Polytechnic University, Hong Kong SAR, People's Republic of China

ABSTRACT

Installing a turbine in a duct generally increases the flow through the rotor. If there is flow confinement due to limited water depth, the presence of lateral boundaries, or the presence of adjacent turbines, a further flow enhancement through the rotor will be achieved. Extensive studies of ducted turbines in uni-directional flow have shown that rotor-based power coefficient C_p can exceed the Betz-Joukowski limit (BJL) for bare turbine, whereas the exceedance of the BJL is rarely reported for duct-area-based power coefficient C_p^* . In this work, CFD studies have been carried out for several flanged duct turbines with different duct geometries under bi-directional flow conditions. The actuator disc approach is used to simulate the rotor. The results show that a flanged duct turbine with an inlet-arc flap and a curved brim can achieve a maximum value of C_p^* close to the BJL for flow from either direction while a symmetric duct turbine gives maximum C_p^* of about 60% of the BJL. The effect of the flow confinement on C_p^* shows C_p^* increases with blockage ratio ϵ and a little variation in the relative performance of ducted and bare turbines. ϵ . The findings pave the way for the realization of turbines with a flanged duct.

ARTICLE HISTORY

Received 26 May 2020
Accepted 1 January 2021

KEYWORDS

Tidal energy; ducted turbine; flanged duct; computational fluid dynamics

Notation

| | |
|------------|---|
| a | Induction factor [–] |
| A | Rotor area [m^2] |
| A_c | Channel cross-sectional area [m^2] |
| A_{duct} | The total projected frontal area of the duct device [m^2] |
| BJL | Betz- Joukowski Limit [–] |
| C_p | Power coefficient normalized with A [–] |
| C_p^* | Power coefficient normalized with A_{duct} [–] |
| C_{ps} | Pressure coefficient [–] |
| C_t | Rotor thrust coefficient/loading coefficient/pressure coefficient [–] |
| D_t | Turbine rotor diameter [m] |
| f | Arc-flap inlet length [m] |
| h | Flange height [m] |
| h_f | Arc-flap inlet height [m] |
| l | Turbulent length scale [m] |
| L | Duct/diffuser length [m] |
| p | Pressure [Pa] |
| p_0 | Reference pressure of the approaching flow [Pa] |
| r | Rotor radius [m] |
| Re | Reynolds number [–] |
| S | Duct exit expanding length [m] |
| t | Duct thickness [m] |
| u | Axial streamwise velocity [m/s] |
| u_τ | Friction velocity [m/s] |

| | |
|------------|-------------------------------------|
| X | Axial distance [m] |
| y | Normal distance to the wall [m] |
| y^+ | Dimensionless wall distance [–] |
| ϵ | Blockage ratio [–] |
| Δ | Relates to change [–] |
| ν | Kinematic viscosity [m^2] |
| ρ | Fluid density [kg/m^3] |
| θ | Duct inlet angle [$^\circ$] |

Subscripts

| | |
|-----|--|
| 0 | Relates to the flow at the inlet of the duct |
| 1 | Upstream of the rotor/disk |
| max | Maximum |

Acronyms

| | |
|----------|--|
| 2D | Two-dimensional |
| 3D | Three-dimensional |
| BEM | Blade Element Momentum |
| CFD | Computational fluid dynamics |
| DES | Detached Eddy Simulation |
| FST | Freestream turbulence |
| LES | Large Eddy Simulation |
| n.a | Not applicable |
| OpenFOAM | Open-source Field Operation and Manipulation |

CONTACT M. Maduka  maduka.maduka@connect.polyu.hk

| | | |
|-------|---------------------------|--------|
| URANS | Unsteady Reynolds-average | Navier |
| | -Stokes | |
| SST | Shear-stress transport | |

1. Introduction

With the aim to reduce human-induced climate change effect and the consideration of a rapid increase in energy price, research on clean energy production is actively promoted. Global investment in renewable energy in 2017 was USD279.8 billion, a 2 percent increase over the previous year (REN21, 2018). Although wind energy is still the major source of clean energy, water flow energy (tidal energy and wave energy) has received attention, and efforts have been put into its commercialization (REN21, 2018). Turbines have been developed a long time ago and are mainly used to extract wind energy. According to Okulov and Van Kuik (2012), analytical study of turbine performance can be traced to Betz and Joukowsky in 1920. One remarkable solution of Betz-Joukowsky limit (BJL) theory is that the maximum amount of power that can be extracted from the fluid flowing through the turbine is $C_p = 16/27$ of the total available flow power, where C_p is called the power coefficient. To increase the value of C_p , the concept of a ducted turbine has emerged in the past several decades. In this design the turbine is placed inside a duct such that the fluid flow will converge towards the turbine and strong vortices will be generated behind the duct resulting in a low-pressure.

Lilley and Rainbird (1956) conducted a one-dimensional analysis and showed that a duct could provide 65 percent more in power compared with that of a bare turbine with the same rotor diameter and the turbine performance is a function of the viscous loss, diffuser exit ratio, and the external shape of the duct. Gilbert and Foreman (1979) succeeded in increasing the fluid flow inside the duct by utilizing several flow slots to control the boundary layer but failed to prevent pressure loss by flow separation. To improve this design, Phillips et al. (1999) developed a multi-slotted duct diffuser to prevent flow separation within the duct. This device was called Vortec 7, but it failed to be commercialized due to an additional requirement of a yawing mechanism and the high cost incurred. Igra (1981) introduced the use of a ring-shaped flap to improve ducted turbine performance. His result showed that using an appropriate ring-shaped flap an 80 percent power augmentation could be obtained while about 25 percent power augmentation was achieved in its inner rear part. Hansen et al. (2000) developed and validated a computational fluid dynamics (CFD) model by modeling the rotor of a wind turbine as an actuator disk. They demonstrated that the BJL could be exceeded

by a factor relative to the fluid flow rate if a mechanism was used to increase the flow rate. Lawn (2003) used one-dimensional theory to analyze the performance of a ducted turbine by treating the parts of the duct upstream and downstream of the turbine as contraction or expansion with specified diffuser efficiencies. Lawn deduced that by choosing a more lightly loaded design a ducted turbine could achieve a 33 percent enhancement in the power coefficient over a bare turbine of the same diameter. For a given duct efficiency, there is an optimum turbine resistance for generating maximum power, because the swallowing capacity of the duct increases as the resistance decreases.

Another concept of the ducted turbine was developed with a flange attached at the exit of the duct called wind-lens (Abe et al., 2005; Abe & Ohya, 2004; Ohya et al., 2008). Their computational results were in good agreement with the corresponding experimental data and showed that the wind speed inside the duct increased by 1.6–2.4 times the approaching wind speed, equivalent to about 4–5 fold power increment compared to the conventional wind turbine. Kardous et al. (2013) carried out numerical simulation, Particle-Image-Velocimetry visualization, and wind tunnel experiments to investigate the effect of the height of flange on wind velocity increase at the inlet section of an empty flanged duct. Their results showed that the presence of the flange alone caused the additional acceleration of the wind of 13 percent to 23 percent. The study, however, neglected the effect of turbine resistance in the airflow and duct interaction. El-Zahaby et al. (2017) studied the effect of the flange angle of a ducted turbine and found that flow acceleration at the entrance of the duct is optimized at an angle of 15° to the normal of the duct with a 5 percent power coefficient increment compared to the duct with a normal flange.

The idea of ducted turbines has been extended in the context of tidal power generation probably inspired by the significant innovations in the performance of ducted horizontal axis turbines in wind turbine technology (Van Bussel, 2007). Also, Edenhofer et al. (2011) reported that horizontal axis tidal turbines are likely to follow a similar development path to wind turbines, where larger capacity turbines will be deployed depending on the progress in finding optimum duct shape (or size), blade design, and turbine array layout. The study of ducted tidal stream devices has been examined by several researchers. Setoguchi et al. (2004) investigated the performance of a turbine in a duct of symmetric shape in a wind tunnel. The duct consisted of diffuser-straight part-diffuser components and brims mounted at both ends of the duct. The case with brim height to rotor diameter ratio of 2.0 showed the best performance

with an increased flow velocity of about 1.3 times the freestream flow velocity. The authors did not consider the case with a turbine present. Shives (2011) used analytical and numerical modeling to study duct of aerofoil longitudinal-section. They found that bare (non-ducted) turbine can produce more power per installed device frontal area. Shives and Crawford (2011) further conducted CFD modeling of several duct designs to gain insight into the effects of viscous loss, flow separation, and base pressure on mass flow increment provided by the duct. The authors found that viscous loss in the inlet is negligible for the cases considered while flow separation and increase in diffuser expansion, inlet contraction, and inner exit angle led to a significant reduction in turbine efficiency. They concluded that it is worthwhile to pursue further study of flanged duct turbines which create a large suction effect downstream. In placing arrays of turbines in a tidal channel, the channel confinement effect should be considered. Garrett and Cummins (2007) found that the maximum power coefficient, $C_{p,max}$ of a bare turbine is proportional to the blockage ratio (ϵ) i.e. $C_{p,max} \propto 1/(1 - \epsilon)^2$, where $\epsilon = A/A_c$ (A and A_c are the rotor area and the approaching flow cross-sectional area respectively). Belloni (2013) carried out a numerical investigation of tidal turbines with symmetric-shape ducts employing the actuator disc model and CFD-BEM (Blade Element Momentum) models. She considered that C_p^* , the power coefficient with the outer area of the duct as the reference area, is a more appropriate parameter for comparison with the power coefficient of a bare turbine. The results showed that the performance of the devices is greatly affected by the blockage ratio and the maximum C_p^* for a ducted turbine is always less than the maximum C_p of a bare turbine. Fleming and Willden (2016)

analyzed turbines in ducts of some symmetric geometries and their results supported the work of Belloni (2013) that the maximum C_p^* of a ducted turbine is less than the maximum C_p of a bare turbine.

For a bare turbine, the BJL caps the theoretical maximum power extracted from the fluid at about 60 percent for a single actuator disc in an unconfined environment and $0.6(1 - \epsilon)^{-2}$ for a confined environment. The BJL has been demonstrated by some researchers (Abe et al., 2005; Hansen et al., 2000; Igra, 1976, 1981) to be exceeded with the introduction of duct to generate significant suction at the duct exit and maintain a large pressure recovery within the duct (Gilbert et al., 1978). However, the demonstrations of performance gain in relation to that of a bare turbine have been questioned as the vast majority of the works used rotor area as the reference area instead of the outer area of the duct as the reference area, as well as the neglect of the effect of the blockage ratio. The maximum values of C_p (rotor area is used as the reference area) and C_p^* (maximum duct cross-sectional area is used as the reference area) for various ducted turbines reported in the literature are listed in Table 1. It shows that only the maximum C_p s are nearly equal to or greater than the BJL while the maximum C_p^* s are all below the BJL. Therefore, the geometric shape of a duct for a turbine with optimum power performance remains unclear. It is reported from the literature that numerous computational, as well as experimental studies, have examined the effect of flange height, diffuser opening angle, hub ratio, and center-body length of the duct (Abe et al., 2005; Abe & Ohya, 2004; Kardous et al., 2013; Mansour & Meskinkhoda, 2014), but to the best of authors' knowledge, there has been no emphasis placed on flanged duct turbines in bi-directional tidal flows.

Table 1. Maximum values of C_p and C_p^* for various ducted turbines.

| Investigators | Type of Ducted Turbine | Blockage ratio, ϵ , and Corresponding BJL | C_p | C_p^* | C_p (bare) |
|----------------------------|---|--|-------|---------|--------------|
| Fleming and Willden (2016) | Bi-directional: | $\epsilon = 0.131$ | 0.82 | 0.46 | 0.85 |
| | B | BJL = 0.784 | 0.85 | 0.48 | |
| | C | | 0.63 | 0.483 | |
| | D | | 0.48 | 0.43 | |
| | E | | 0.60 | 0.45 | |
| Belloni (2013) | Bi-directional | $\epsilon = 0.035$ BJL = 0.644 | 0.63 | 0.42 | 0.63 |
| | Bi-directional | $\epsilon = 0.2$ BJL = 0.938 | 0.94 | 0.62 | 0.90 |
| | Open-center | $\epsilon = 0.035$ BJL = 0.644 | 0.59 | 0.39 | 0.63 |
| Shives and Crawford (2011) | Scaled NaCA0015 aerofoil (D ₇) | $\epsilon = 0.03$ BJL = 0.638 | 1.10 | 0.38 | 0.58 |
| Ohya et al. (2008) | Flanged diffuser ($L/D = 1.25; h/D = 0.5; \theta = 4^\circ$) | n.a (open-type test section) | 1.38 | 0.21 | 0.26 |
| Abe and Ohya (2004) | Flanged diffuser ($L/D = 1.25; h/D = 0.35; \theta = 15^\circ$) | $\epsilon = 0.011$ BJL = 0.606 | 1.30 | 0.32 | 0.60 |
| Hansen et al. (2000) | NaCA0015 aerofoil(deformed) | $\epsilon = 0.0041$ BJL = 0.605 | 0.94 | 0.51 | 0.59 |
| Igra (1981) | Shroud with ring-shaped flap (NACA 1412) | n.a (pilot-plant exposed to the atmosphere) | 1.79 | 0.45 | 0.74 |

Ohya et al. (2008) showed that the shape of the duct largely determines the streamlined velocity through the duct while Abe and Ohya (2004) pointed out that the performance of a flanged duct strongly depends on whether separation occurs within the diffuser. Thus, in this work, several carefully designed flanged duct tidal turbines with different duct shapes (symmetric and asymmetric) for both uni-directional flow and bi-directional flow will be investigated numerically to explore the power augmentation and the possibility of exceedance of BJL for C_p^* . Further analysis of the influence of blockage ratio on the performance of ducted turbines will also be conducted.

2. Numerical simulation details

2.1. Modeling of the turbine

Actuator disc models have been applied to tidal current turbines (Garrett & Cummins, 2007; Houlsby et al., 2008; Whelan et al., 2009). Garrett and Cummins (2007) considered a tidal turbine in a rigid-lid channel. Whelan et al. (2009) included the deformation of the free surface while Houlsby et al. (2008) carried out a similar analysis with the inclusion of downstream mixing unlike Whelan et al. (2009). Generally, the models assume that changes in the axial velocity of the flow dominate and that crossflow velocities may be neglected. Increasing blockage improved turbine performance, resulting in higher thrust and power coefficients over a larger range of tip-speed ratios (Garrett & Cummins, 2007; Houlsby et al., 2008; Kolekar & Banerjee, 2015; Ross & Polagye, 2020; Whelan et al., 2009). Whelan et al. (2009) obtained a good approximation for a highly blocked flow pass tidal stream turbines near the free surface with the experimental tests. They concluded that agreement between the effects of free surface proximity and blockage with experiment should improve further as the blockage is reduced. Consul et al. (2013) demonstrated that the effects of rigid-lid and free-surface deformation on the power of a crossflow tidal turbine to be negligible particularly for blockage conditions less than or equal to 0.25. Kolekar and Banerjee (2015) investigated the effect of blockage on turbine performance characteristics using CFD analysis. Results showed that turbine performance generally increases with increasing the blockage ratio. No blockage corrections are necessary for blockage ratios less than or equal to 0.11 when compared to the unblocked case. Also, the performance with tip-speed ratios less than 4 was found to be weakly dependent on the blockage ratio. For instance, as the tip-speed ratio increases from 1.46 to 2.93, a 6 percent increase in C_p from blockage ratio of 0.042 to 0.42 was observed. However, the impact of

blockage ratio on performance curves is significant with tip-speed ratios greater than 4. The peak C_p increased from 0.32 to 0.46 for the blockage ratio increased from 0.042 to 0.42. On the effect of boundary proximity, their experimental investigation suggested for optimum performance in a confined system, the turbine rotational disc should be at least one radial distance away from the solid channel wall and half radial distance below the free surface. Ross and Polagye (2020) experimentally examined the effects of blockage on the performance of a crossflow and an axial-flow turbine. Both turbines were characterized by conditions of high blockage and negligible blockage while other significant parameters were held approximately constant. Overall, the effects of increased blockage ratio increase the turbine's power performance just as in previous studies. However, error associated with blockage corrections is turbine geometries or test conditions specific.

In the present numerical simulation, the solver employed is OpenFOAM (Greenshields & Openfoam, 2016), a free Open-source CFD software package based on the finite volume method. The turbine is modeled as an actuator disc, the swirl and shedding of coherent vortices from the blades are not accounted for. This assumption may not be accurate if the turbines are close together as interaction among turbines may exist due to the swirling motion of blades. More so, the inflow cross-sectional area is a circle and the actual shape of the inflow cross-section is assumed unimportant. This requires that the cross-sectional area is significantly larger than the cross-sectional area of the rotor, and the effect of the free-surface boundary should not be important. To meet these conditions a relatively small blockage ratio is required. Nishino and Willden (2012a) showed that the influence of the aspect ratio is secondary to blockage ratio when considering the efficiency of an array of turbines installed in a large rectangular tidal channel. Thus, the computation domain and the channel containing the turbine in the present simulation are assumed to be axisymmetric, which implies that the effects of free surface deformation, supporting structure and channel cross-section are negligible. The turbine region is discretized by unstructured grids around the rotor and structured grids upstream and downstream of the turbine. With the domain size normalized by the turbine diameter, $D_t = 20m$, the inlet, and outlet were $5D_t$ upstream and $10D_t$ downstream of the duct respectively. Simulation results for the case with longer domain length ($20D_t$) downstream of the duct are less than one percent difference with the corresponding simulation results for the domain with $10D_t$ downstream length, so the use of $10D_t$ downstream length is deemed adequate for the present study (Figure 1). The boundary conditions used are constant velocity, $u_0 = 2.0m/s$

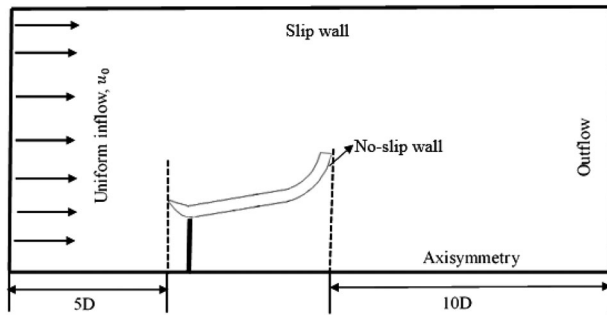


Figure 1. Computational conditions and boundary conditions.

at the inlet, zero-gradient at the outlet, slip wall at the top, and no-slip wall with wall function treatment at the duct wall. For wall function treatment (appropriate for high Reynolds number flow), the dimensionless distance, $y^+ (= u_\tau y/\nu$, where u_τ is the friction velocity, y is the normal distance to the wall, ν is the kinematic viscosity of fluid) in the range $30 \leq y^+ \leq 300$ was set.

The fluid is water of density $\rho = 1000 \text{ kg/m}^3$ and kinematic viscosity $\nu = 10^{-6} \text{ m}^2/\text{s}$, resulting in the Reynolds number $Re = 4 \times 10^7$ (length scale used is the turbine diameter, D_t). The freestream turbulence intensity (FST) of 10 percent and turbulent length scale of $l = 0.1D_t$ were used in computing freestream inflow turbulence parameters. Also, a low freestream turbulence intensity of 0.1 percent was tested for the case of a bare turbine (Fleming & Willden, 2016; Nishino & Willden, 2012b). Table 2 shows the details of the simulation scheme. The turbine is treated as an actuator disc with the wake swirl and discrete blade effects neglected (Belloni, 2013; Fleming & Willden, 2016; Rahman et al., 2018; Shives & Crawford, 2011). In the numerical model, the axial resistance induced by the actuator disc was represented by a pressure drop Δp across the disk,

$$\Delta p = \frac{1}{2} \rho u_0^2 C_t \quad (1)$$

where C_t is a pressure coefficient or load coefficient, and

$$C_p = C_t \frac{u_1}{u_0} \quad (2)$$

where C_p is the power coefficient using the rotor area as the characteristic area; and u_1 is the spatially averaged velocity at the rotor. Another power coefficient C_p^* can be defined using the area swept by the outer diameter of the duct A_{duct} :

$$C_p^* = \frac{A}{A_{duct}} C_p \quad (3)$$

Table 2. Details of numerical simulation.

| | |
|---------------------------------------|--------------------------------------|
| Computational grid | Mixed (structured and unstructured) |
| Scheme | Finite volume method |
| Time advancement method | Euler |
| Discretization of the convective term | 2 nd -order upwind scheme |
| Coupling algorithm | pimpleFOAM |
| Reynolds number | 4×10^7 |

Note that for bare turbine there is no duct and $A_{duct} = A$, $C_p^* = C_p$. The induction factor a is defined by

$$a = 1 - \frac{u_1}{u_0} \quad (4)$$

A negative value of a refers to the condition that the velocity of flow through the rotor is accelerated and greater than the ambient velocity. In OpenFOAM, the pressure-jump Δp in Equation (1) is specified by using the utility function ‘createBaffles’.

The use of an actuator disc to simulate a turbine has the advantage that there is no need to resolve the blades explicitly and the number of grid points can be reduced significantly. Computational efficiency is important as there are a lot of scenarios to be simulated for various ducted turbines. The actuator disc imposes a streamwise resistance only and extracts the upper bound power from the flow. Additional losses due to swirl and shedding of coherent vortices from the blades are not accounted for. Furthermore, specific rotor design may be required for each duct for optimum performance. For a fair and straightforward comparison of duct performance, the assessment of the upper bound power extraction by the ideal rotor (actuator disc) is preferable. (Fleming & Willden, 2016; Shives & Crawford, 2010). All meshes were generated using Gmsh 3.0.6 (Geuzaine & Remacle, 2009) and imported into OpenFOAM using the conversion utility command, ‘gmshToFoam’.

The turbulence model employed is the $k - \omega SST$ (shear-stress transport) model which is able to predict separation in adverse pressure gradient generally occurred along the entire duct surface (Menter et al., 2003; Shives & Crawford, 2011). The performance of the $k - \omega SST$ turbulence model in predicting flow separation has been extensively studied in the literature and is the most preferred turbulence model used in several ducted tidal turbine studies (Belloni, 2013; Fleming & Willden, 2016; Shives & Crawford, 2011). A comprehensive summary of the superiority of $k - \omega SST$ turbulence model in predicting complex flows was presented in Shives and Crawford (2011). The pimpleFOAM (merged PISO-SIMPLE), a robust and efficient transient solver was then used in solving the incompressible unsteady Reynolds-average Navier-Stokes (URANS) equations. A literature review on URANS is presented in

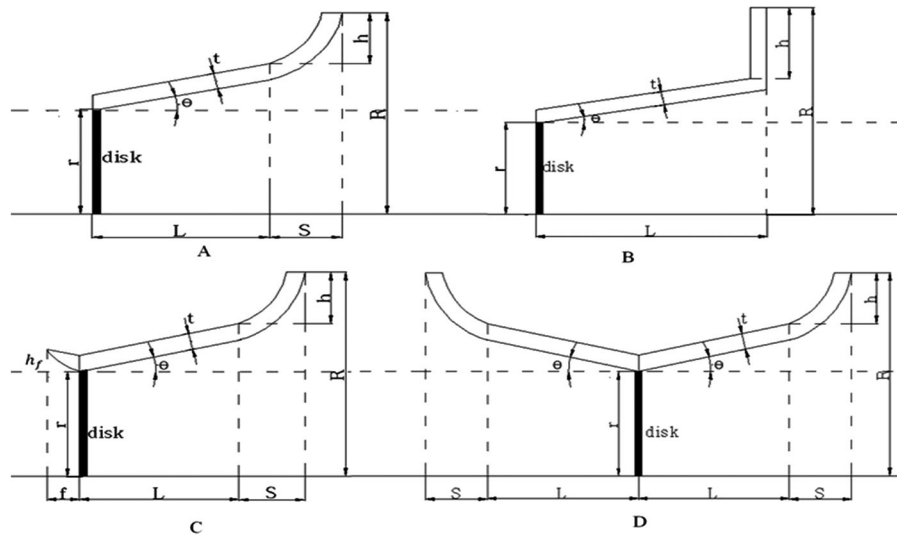


Figure 2. Duct geometries for cases with (A) curved flange (B) vertical flange (C) curved flange with inlet-arc flap (D) curved flanges at inlet and outlet. Not to scale.

section 2.3. Throughout the simulation Courant number less than unity was maintained to ensure stability. The post-processing of the results was performed using Paraview 5.3.

2.2. Choice of duct shapes

Two types of ducts are carefully chosen. The first three ducts are of asymmetric shape (Type A, B, C) and the fourth duct is of symmetric shape (Type D), as shown in Figure 2. Asymmetric shape ducts are commonly used for a ducted turbine in unidirectional flow. Their performance in bi-directional (tidal) flow is however seldom been studied. Symmetric shape ducts are always used in bi-directional (tidal) flow as their performance is independent of the direction of flow. Type B is the design used in Ohya et al. (2008) for unidirectional flow. The vertical flange at the outlet is used to increase the suction in the wake and to generate a larger flow within the duct. This duct is primarily used for unidirectional flow but its performance in bi-directional (tidal) flow will be investigated.

Type A is an improved design with a curved flange. It aims to produce better flow behavior and less head loss under reversed flow conditions. For Type C duct, a small inlet-arc flap is added to improve the inlet flow condition and reduce the inlet head loss. Type D is symmetrical and consists of a Type A duct and its mirror image. Its performance will be identical for flow from both directions. In all cases, the duct thickness, $t = 0.025D_t$, rotor radius $r = D_t/2 = 10$ m resulting in $R/r = 1.31$ (where R is the duct radius) and position of the rotor $X/D_t = 0$. The geometric parameter of the duct is $L/D_t = 0.25$ and the flange

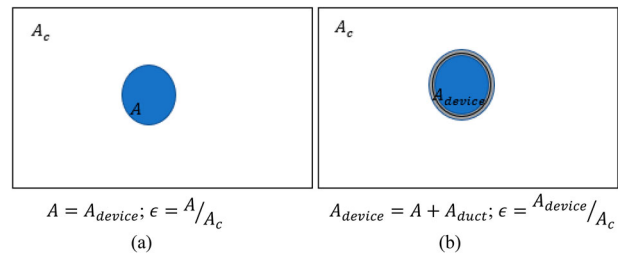
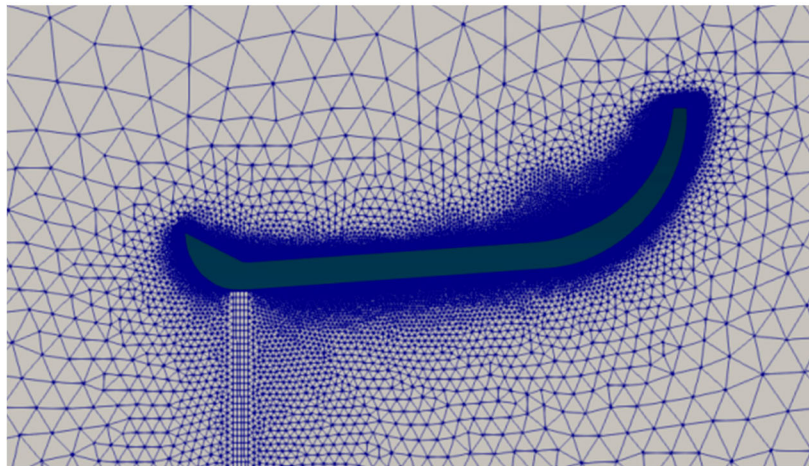


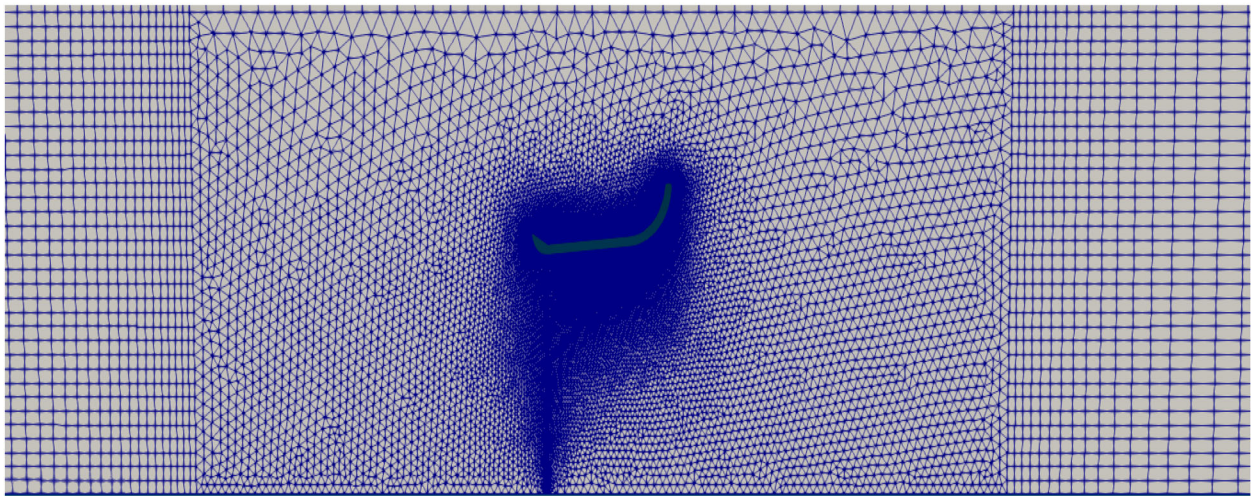
Figure 3. Blockage ratio, ϵ definition for (a) bare (b) ducted turbines.

length to duct diameter ratio is $h/D_t = 0.1125$. The inlet-arc flap length and height were set to $f = 0.05D_t$ and $h_f = 0.05D_t$, the length between the duct length and the flange periphery is $S = 0.125D_t$ (specifically for Type A and C duct types) and the inlet angle was set to $\theta = 4^\circ$. The choice of these values is based on a preliminary parametric study together with the results from previous works (Abe & Ohya, 2004; Ohya et al., 2008). The blockage ratio was set at $\epsilon = 0.131$ unless otherwise mentioned for comparisons with previous works (Fleming & Willden, 2016). Figure 3 illustrates the definition of blockage ratio (ϵ). In the simulation, the outer rectangular region is replaced by a circular region of the same area as the simulation is axisymmetric. In the study, the blockage ratio was kept to a maximum of 0.131 and the effect of changing the outer boundary is considered small.

The grid used in the CFD simulation is carefully chosen to satisfy the wall function requirements. A typical grid layout used in the simulation is shown in Figure 4. Grid convergence tests following the procedures recommended by the Fluid engineering Division of ASME (Celik et al., 2008) have been conducted with Type C



(a)



(b)

Figure 4. Typical grid layout (a) around the duct and turbine (b) before and beyond the duct and turbine.

Table 3. Grid convergence tests for Type C ducted turbine (with $C_t = 1.05$, $L = 0.25D_t$, $h = 0.1125D_t$, $f = 0.05D_t$, $S = 0.125D_t$ & $\epsilon = 0.131$).

| Grids | No of cells | C_p | C_p^* |
|--------|-------------|--------|---------|
| Coarse | 26172 | 1.3540 | 0.7886 |
| Medium | 104688 | 1.2521 | 0.7293 |
| Fine | 418752 | 1.2256 | 0.7139 |

ducted turbine. Some details about the grids used and the computed results of interest, C_p (or C_p^*) are shown in Table 3.

For the solutions, the order of convergence was obtained to be approximately 2. The grid convergence index for the medium grid and the fine grid was computed to be 0.95%. Figure 5 shows the sensitivity of computed C_p with grid size. Since the objective is to select the most appropriate mesh that will give acceptable results in less computational time, the medium grid was used in the subsequent simulations.

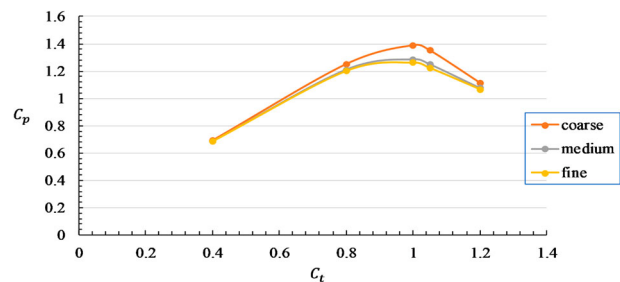


Figure 5. Sensitivity of C_p with grid size.

2.3. URANS model with $k - \omega$ SST turbulence closure

The flow field around a flanged duct turbine is characterized as a typical bluff-body flow field with highly complex and unsteady aerodynamic and/or hydrodynamic phenomena: separation and re-attachment of the shear layer along the internal walls of the duct, vortex shedding from the flange in the external flow around the duct and mixing of the internal and external flows at the

outlet of the duct. The focus of this study is to investigate the performance of flanged duct turbines under bi-directional flow and propose an optimum design. Noting that turbulence is a time-dependent 3D process whose computational simulation is particularly challenging. Among the two-equation RANS models based on Boussinesq approximation, the URANS model with $k - \omega SST$ turbulence closure was adopted in the present study. The $k - \omega SST$ model allows for direct integration through the boundary walls and shows superiority for wall simulation as previously stated. Although 3D LES (Large Eddy Simulation) or DES (Detached Eddy Simulation) is preferred to study the complex 3D flow around a bluff-body, Sun et al. (2009) demonstrated through simulation that 2D URANS solution contains 3D effect and is physical. Several other authors have extensively examined the practical applicability of the URANS $k - \omega SST$ approach. Sun et al. (2009) employed 2D URANS model with $k - \omega SST$ turbulence closure to predict the motion-induced aerodynamic forces of a rectangular section with $B/D = 4$ (where B is the cross-sectional width and D is the section depth) at a reasonable computational cost; also the effect of the freestream turbulence was studied. A similar study was carried out by Nieto et al. (2015) using OpenFOAM. Their result also proves that 2D URANS model with $k - \omega SST$ turbulence closure can adequately model fluid-structure interaction responses, avoiding time-consuming 3D LES simulations or the development of in-house sophisticated software. Stringer et al. (2014) conducted URANS computations of flow around a circular cylinder for a wide range of Reynolds numbers. OpenFOAM was one of the solvers used. The simulation was 2D and the $k - \omega SST$ turbulence closure was employed. The computed results were close to the experimental data in terms of coefficients of lift, drag, and vortex shedding frequency at the subcritical Reynolds number range. Stringer et al. (2014) further suggested using pimpleFOAM, a solver capable of outer

loop time-stepping may improve high Re convergence in OpenFOAM.

For the present problem, the flow is generated by the actuator disc which creates a pressure drop across the disc. The effect of the duct is to divert more flow towards the disc. Flow separation and vortex shedding from the duct exerts a secondary effect on the flow through the disc. The URANS model with $k - \omega SST$ turbulence closure is considered to be a viable tool for the problem. Details about the model verification are described in section 2.4.

2.4. Model verification

The first case is to simulate a bare turbine in a confined channel. The computed power coefficient, C_p is compared with the corresponding power coefficient obtained from the actuator disk theory under confined flow. For this purpose, the blockage ratio of the channel is set to $\epsilon = 0.108$ leading to $C_{p,max} = 0.7448$ (Garrett & Cummins, 2007). With all flow field residuals (velocity and pressure) set to 10^{-6} , the simulations were performed with a transient solver and proceeded with a time step size of 0.0001s. Results were then evaluated by comparing the time-averaged flow fields and the value of the power output coefficients (Eqs. 2 & 3). The results are shown in Figure 6. It can be observed that the computed results for the low freestream turbulence (Low FST) case match the theoretical results closely. The increase of FST to 10% (High FST) increases the strength of turbulent mixing downstream of the turbine and increases the power generation and hence the coefficient C_p . In the present case with $\epsilon = 0.108$, the increase in the maximum power output is about 8%. The present actuator disk validation results are qualitatively similar to those of Fleming and Willden (2016). The model was then applied to simulate the flow through the wind lens of Abe and Ohya

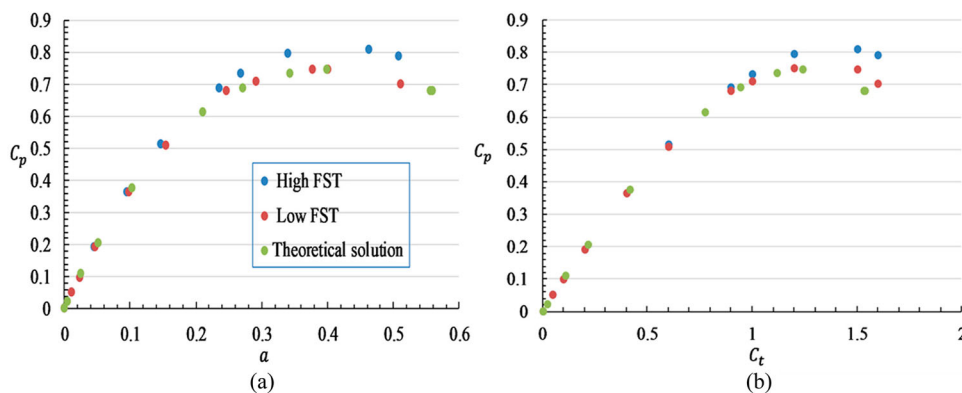


Figure 6. Effect of freestream turbulence on C_p with (a) a (b) C_t for a bare turbine with $\epsilon = 0.108$.

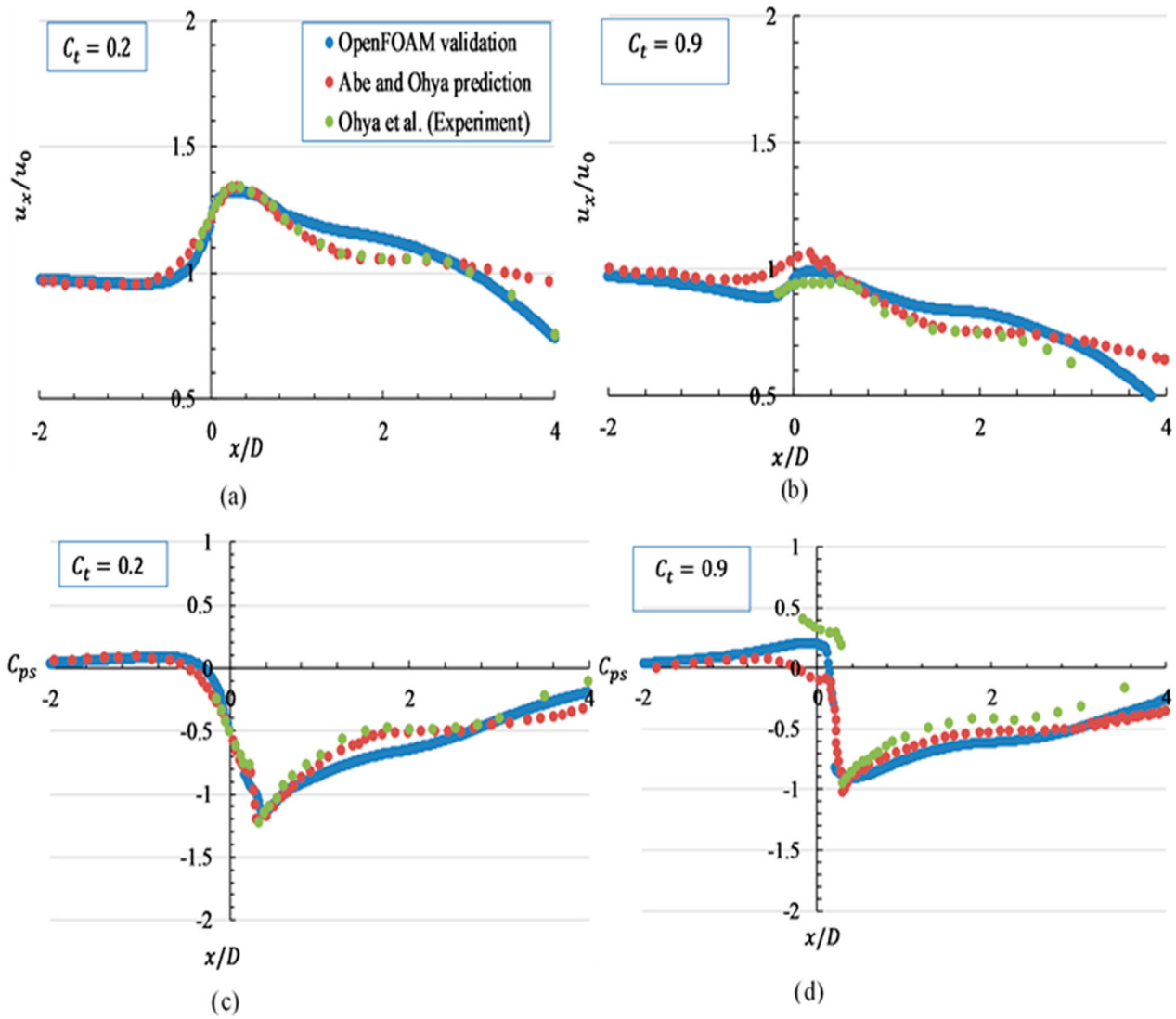


Figure 7. Axial distributions of streamwise velocity ratio (a) $C_t = 0.2$ (b) $C_t = 0.9$ and pressure coefficient (c) $C_t = 0.2$ (d) $C_t = 0.9$.

(2004), Type B duct in Figure 2, for two loading conditions: $C_t = 0.2$ and $C_t = 0.9$. The computed variations of pressure coefficient C_{ps} and normalized velocity profiles along the centerline are shown in Figure 7. The pressure coefficient is defined as $C_{ps} = (p - p_0)/(0.5\rho u_0^2)$, where p is pressure, and p_0 is the reference pressure of the approaching flow. It can be observed that the computed centerline pressure coefficient profiles and the computed centerline velocity profiles matched well with the corresponding experimental measurements by Abe and Ohya (2004). The present $k - \omega SST$ turbulence model predicted accurately the peak pressure coefficient and the peak velocity ratio for both cases, while the $k - \varepsilon$ turbulence model (Abe & Ohya, 2004) slightly overpredicted the peak velocity ratio and underpredicted the peak pressure coefficient for the case of $C_t = 0.9$. In the far wake region ($x/D > 3$) the decreasing trend before the recovery of pressure and velocity are predicted very well by

the present $k - \omega SST$ model. In the near wake region ($x/D < 3$) the $k - \varepsilon$ turbulence model gives a better prediction of the profiles. The inaccuracies in the simulations may be due to the errors in the experimental measurements, the errors incurred in the turbulence models, and the errors in the grid discretization.

3. Results

3.1. Power coefficients

Extensive CFD simulations have been carried out for the preliminary parametric study. The optimum geometrical parameters of the duct obtained are listed in section 2 and repeated here: $L/D_t = 0.25$, $h/D_t = 0.1125$, $f/D_t = 0.05$, $S/D_t = 0.125$, $\theta = 4^\circ$. The criteria for choosing this set of parameters are based on the power output performance and the practicability in the realization of the duct.

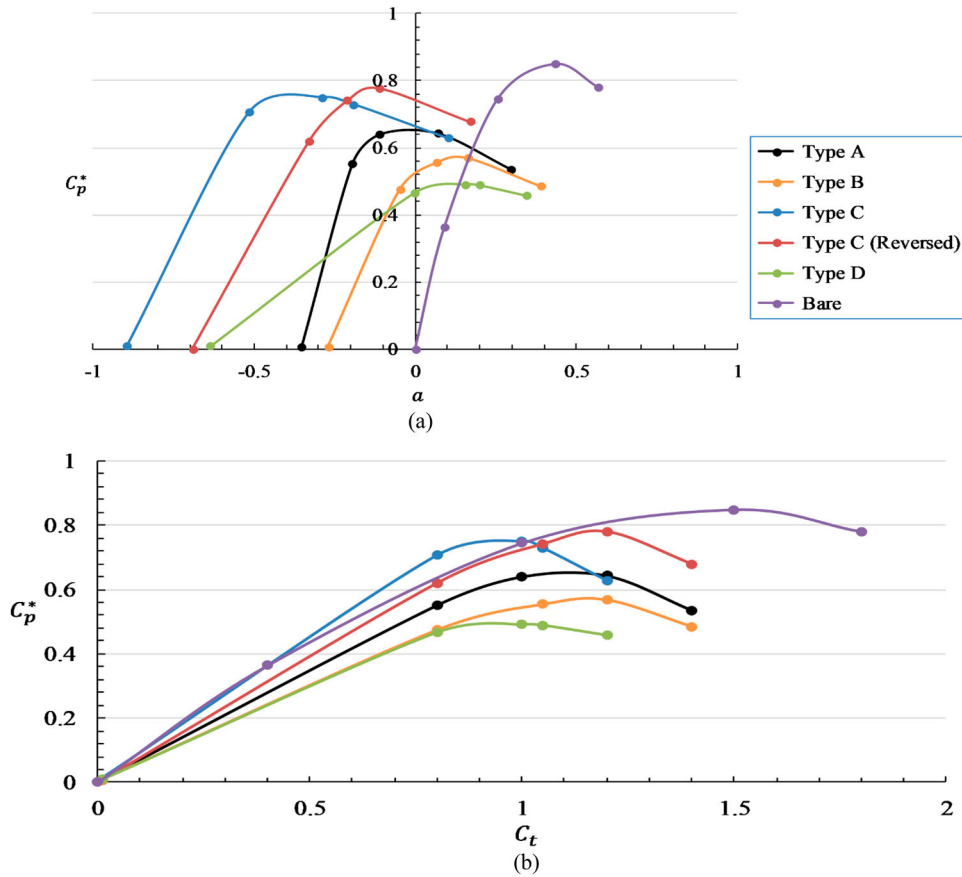


Figure 8. Variation of C_p^* with (a) a (b) C_t (C_t ranges from 0 to 2).

Also, the effects of duct length and flange height variations for Type B duct have been previously reported in Abe and Ohya (2004). In all cases, the rotor area is the same, and simulations are run at least for five different values of C_t . The power coefficients for the ducted devices are represented by C_p^* and C_p with different reference areas.

The power coefficient C_p^* is plotted as a function of the axial induction factor, a and thrust coefficient, C_t for duct Type A, Type B, Type C, Type C (Reversed), Type D, and the bare devices in Figure 8. It can be seen that the asymmetric duct design (C and reversed C) show a significant improvement in power output reaching a peak value of approximately 0.8 compared to the bare device of about 0.85, whereas the symmetric duct design D attains a maximum power output of about 0.5, which is similar to that obtained from the best performing symmetrical duct designs by Fleming and Willden (2016). This significant improvement achieved by Type C duct design can be attributed to the additional flow recirculation created behind the duct device as a result of the incorporation of a flange at the exit of the duct thereby inducing a low-pressure effect (Abe & Ohya, 2004; Ohya et al., 2008; Setoguchi et al., 2004). Flow separation occurred at the

tip of the flange, a low-pressure region was created downstream of the flange, which drew more flow into the duct due to larger pressure difference across the inlet and outlet of the duct. Also, the inlet-arc flap and the curved-nature of the flange smoothly channel the flow into and out of the duct device. It reduces or avoids separation of flow on the near-wall region inside the duct device and downstream, in contrast to the duct equipped with a vertical flange at the exit (Abe & Ohya, 2004). The velocity field and pressure field of the flows will be further discussed in section 4.2. The optimal performance of this duct device is however achieved at lower loading conditions ($C_t < 1.2$) and decreases with C_t for C_t exceeding 1.2. This is due to flow deceleration caused by the flow separation inside the duct device and the build-up of the recirculation region limiting wake expansion.

The variation of the power coefficient C_p (adopting the rotor area as the reference area) with the induction factor a and thrust coefficient, C_t are shown in Figure 9. The peak C_p of Type C ducted turbine is about 1.6 times of that of the bare turbine while the peak C_p of the Type D symmetric ducted turbine is merely close to that of the bare turbine. The magnitude of the pressure gradient increases with the size of the flange up to a certain

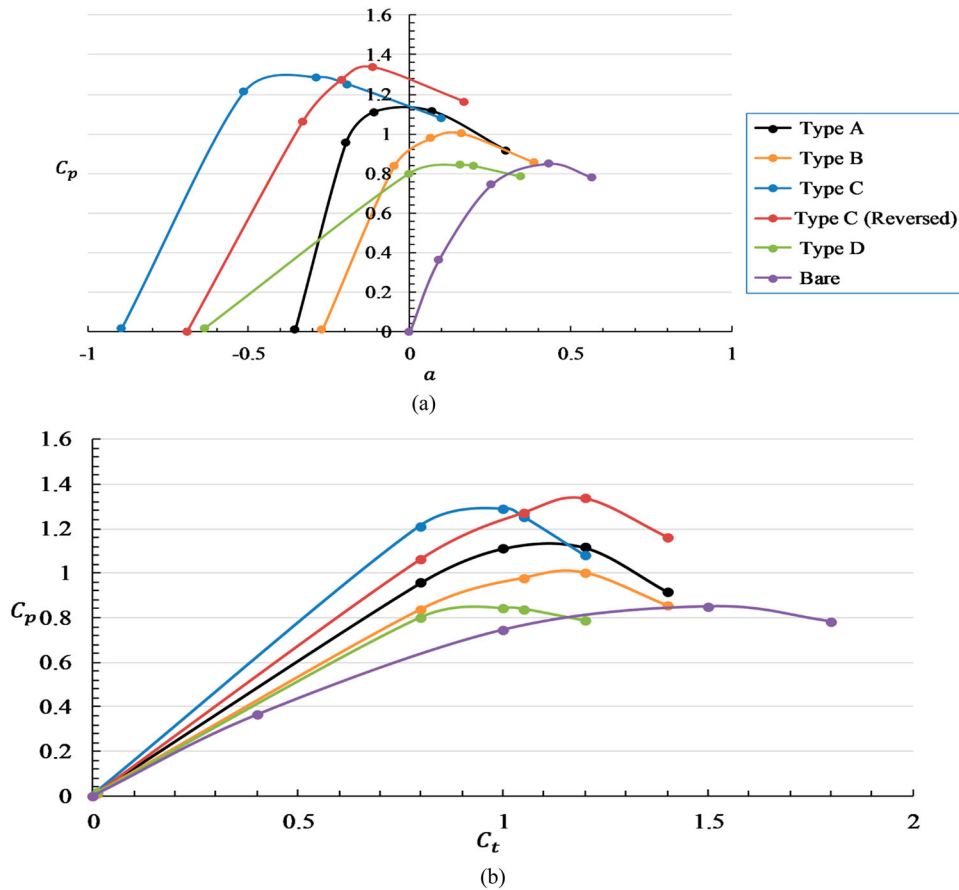


Figure 9. Variation of C_p with (a) a (b) C_t (C_t ranges from 0 to 2).

size. Further increase in flange size will introduce a blocking effect restricting the flow into the duct (Ohya et al., 2008). Therefore, C_p increases with flange size up to a certain value. Generally, the increase in velocity through the rotor is offset by the decrease in the ratio of A/A_{duct} , resulting in a decrease of C_p^* with an increase in flange size.

3.2. Flow characteristics

To investigate the flow characteristics of various turbines, the computed flow streamline colored with velocity normalized by the inflow velocity at or close to the maximum power output conditions are shown in Figure 10. Similar upstream flow behavior is observed for each of the devices. Differences arise as the incident flow impinges just on the rotor and downstream of the rotor. For the bare case, the velocity decreases as the flow approaches the rotor and gradually expands further downstream of the rotor wake (Figure 10a). For Type A duct, flow recirculation from the flange occurs in the external flow. As a result, a high-speed flow develops just downstream of the rotor but is counteracted by boundary-layer flow separation along the internal walls of the duct. Further

downstream, the high-speed flow quickly dies out forming a recirculation wake profile at a lower thrust coefficient ($C_t = 1.0$) and eventually expands (Figure 10b). Similar to Type A duct, flow recirculation from the flange in the external flow occurs in Type B duct (Figure 10c). Although no separation occurs along the internal walls of Type B duct, the Type A duct demonstrates the expanding curved flange not only generates a low-pressure region behind the duct peculiar to flanged duct devices for increasing flow swallowing capacity but also align and channels the flow out of the duct, hence, a greater flow rate. This is a consequence of the increase in the aforementioned duct performance presented in Figures 8 and 9. For Type C duct equipped with a curved inlet-arc flap ensures that no separation occurs along the inner boundary walls of the duct as it streamlined the flow into the rotor plane and along the duct walls. Also, the presence of the expanding curved flange at the periphery of the duct easily align and channels the flow out of the duct while still generating a low-pressure region behind the duct. This inherent simultaneous action led to a significant increase in flow swallowing and transmission capability of the duct entailing a larger low-pressure zone (Figure 10d and Figure 11d). A higher-speed flow

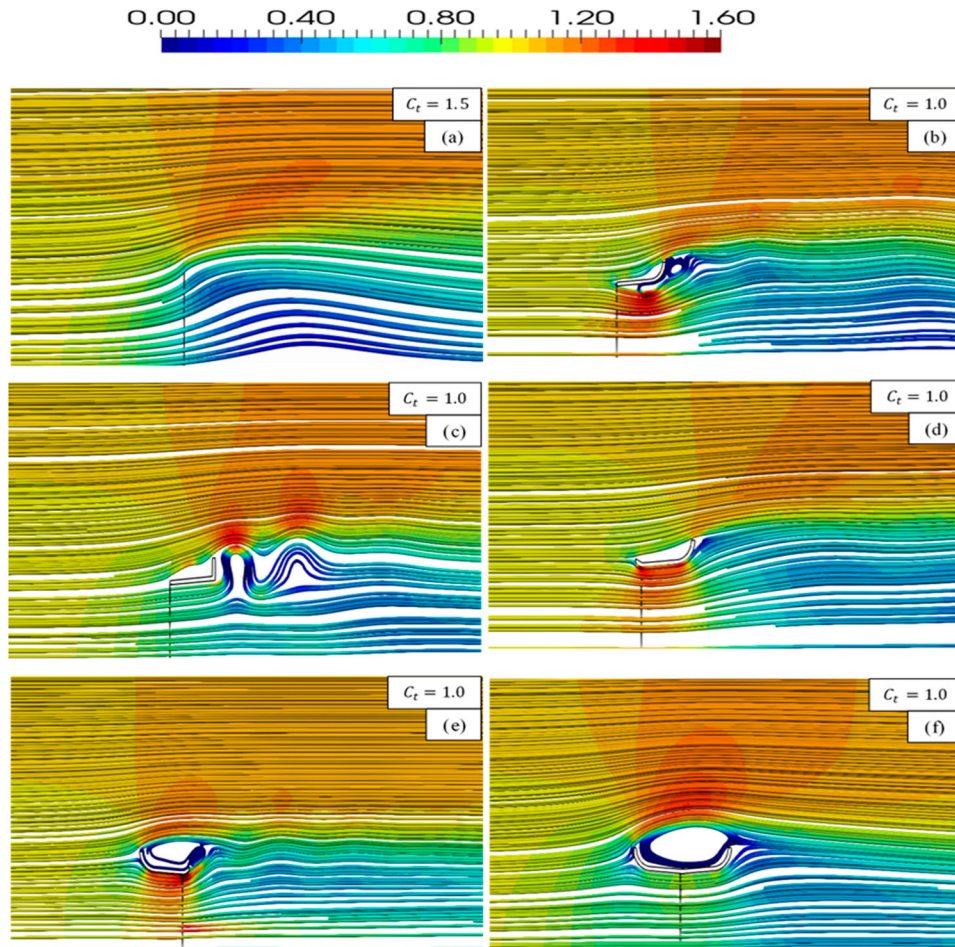


Figure 10. Flow streamlines for (a) Bare (b) Type A (c) Type B (d) Type C (e) Type C Reversed (f) Type D. Flow direction is from left to right. Color denotes normalized velocity magnitude.

concentration is seen around the rotor and downstream of the duct just before the duct exit, unlike Type B with a slightly less velocity spread around the rotor. Similar behavior is observed in the reserved case (Type C Reversed) where the curved inlet-arc flap served as the duct flange (Figure 10e). This further shows that a curved flanged type is preferred and hence, the best performing duct type (see Figures 8 and 9). For the Type D duct, the front curved flange generates a large recirculation zone just outside the duct (Figure 10f). The recirculation bubble diverts more flow outside the duct and results in a lower flow rate through the rotor. It should be noted that for the ducted turbines the peak power coefficient occurred at the loading condition with the thrust coefficient significantly smaller than that of a bare turbine. Also, the incorporation of the inlet-arc flap and the shape of the inlet-arc flap and flange is a strong determinant of the nature of the flow inside and around the duct and downstream.

The pressure fields of various ducted turbines at or close to the maximum power output conditions are shown in Figure 11. For the bare case (Figure 11a), a

pressure rise occurs in front of the rotor. This limits the approaching flow (at zero pressure) through the rotor. For Type A duct (Figure 11b), a slight pressure rise occurs in front of the rotor but counteracted by the action of the curved flange which diverts more flow into the duct.

For Type B duct (Figure 11c), the pressure rise is of a lesser extent due to the vertical flange which creates a lower pressure zone downstream. For Type C (Figure 11d), no pressure rise occurs in front of the rotor (unlike Type A) and a suction zone occurs just downstream of the rotor. A larger flow thus is resulted. For Type C reversed duct (Figure 11e), a slight pressure rise occurs. This is counteracted by the action of the curved flange which diverts more flow into the duct. For Type D duct (Figure 11f), the recirculation bubble just outside the duct is larger than that of Type C reversed. The downstream part of the duct with curved flange shelters the rotor and causes the low-pressure zone to occur further downstream of the rotor, resulting in a lesser flow rate.

The variation of streamwise velocity ratio and pressure coefficient along the centerline for Type C and

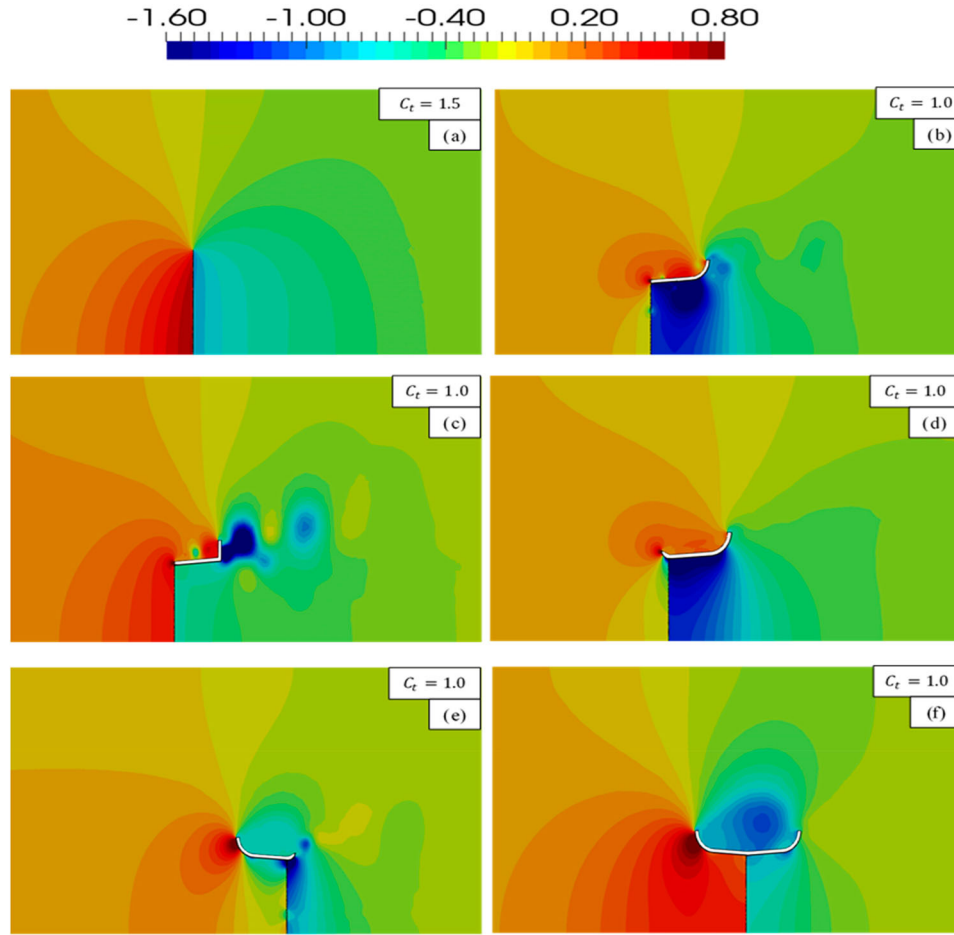


Figure 11. Pressure fields for (a) Bare (b) Type A (c) Type B (d) Type C (e) Type C Reversed (f) Type D. Flow direction is from left to right.

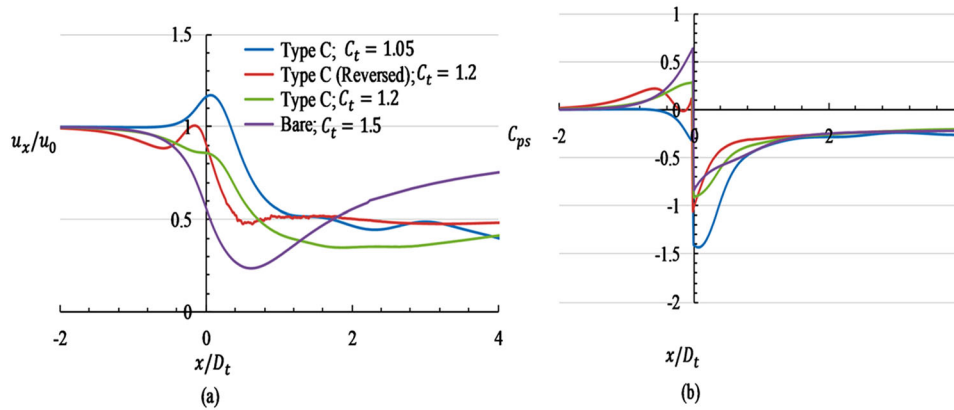


Figure 12. Axial distributions of streamwise (a) velocity ratio (b) pressure coefficient for bare and Type C ducted turbine.

bare turbines are shown in Figure 12. At the location of peak power coefficient, the pressure coefficient just downstream of the rotor is the lowest, corresponding to $C_t = 1.05$ for Type C duct, $C_t = 1.2$ for Type C reversed duct. A peak velocity also occurs just upstream of the rotor. When the loading condition shifts away from that producing the peak coefficient, the peak velocity decreases and can be lower than the approaching velocity

(case with $C_t = 1.2$ for Type C duct), and also the value of the lowest pressure increase.

3.3. Effect of blockage ratio

In placing arrays of turbines in a tidal channel more flow will be drawn into the turbines due to flow confinement from adjacent turbines. Garrett and Cummins

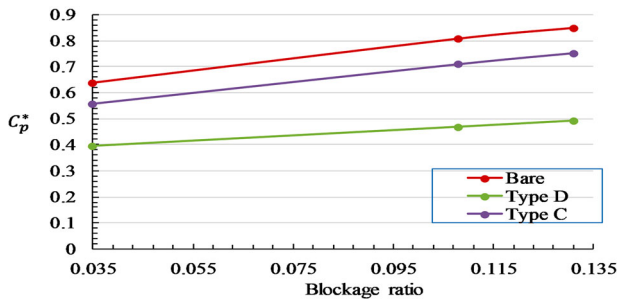


Figure 13. Variation of C_p^* with blockage ratio for bare, Type C, and Type D turbines.

(2007) have developed an analytical model to study the effect of flow confinement on the flow through a bare turbine. The effect of the blockage ratio on the peak power coefficient of the ducted turbines is studied by using CFD. Figure 13 shows the variation of the maximum power coefficient (in terms of C_p^*) with the blockage ratio. As stated in section 1, the blockage ratio is defined to be the cross-sectional area of the rotor divided by the cross-sectional area of the flow bounded by adjacent turbines or solid boundaries. It is observed that the maximum power coefficient increases with the blockage ratio and reaches a value of 0.78 when the blockage ratio is 0.131 (Garrett & Cummins, 2007). For a higher blockage ratio, the interaction between adjacent turbines may be significant and the inlet velocity may become nonuniform. This is beyond the scope of the study of the present work.

In the present computation, the height of the channel is varied such that the required blockage ratio is achieved. The blockage ratio varies from 0.035 (relatively unblocked) to 0.131 chosen from related past studies (Belloni, 2013; Fleming & Willden, 2016). The results for Type C and Type D turbines are shown in Figure 13. In all cases the peak C_p^* increases with blockage ratio. The bare turbine consistently gives the highest C_p^* for a given blockage ratio, as the rotor size is increased and set equal to the duct size for the other cases. The relative performance of duct turbines varies little with the blockage ratio, with Type D turbine giving the least rate. For Type C turbine, its C_p^* is 88% of the corresponding C_p^* of bare turbine over the range of blockage ratio covered. For Type D turbine, its C_p^* slightly varies from 62% of the corresponding C_p^* of bare turbine at blockage ratio 0.035 to 58% at blockage ratio 0.131.

4. Conclusions

A turbine with a flanged duct has been identified to give a significant improvement in power output performance for tidal flow based on CFD simulations. The duct has

a curved flange at the rear end to increase the pressure drop in the wake region for forward flow and increase the approaching velocity by converging the flow into the duct. It also has a flap at the front end to reduce the inlet loss for forward flow and outlet loss for reversed flow. The maximum power coefficient C_p achieved is over 60% higher than that of a bare turbine if the rotor area is used as the reference area. The maximum power coefficient C_p^* is close to that of a bare turbine if the largest projected area with flange is used as the reference area. The effect of blockage ratio on power coefficients is examined. In all cases, the power coefficients increase with blockage ratio while the relative performance of ducted turbines compared with the bare turbine varies little with blockage ratio.

For bare turbines, the power coefficient is capped by the BJL. Installing duct diffuser will increase C_p such that the BJL is exceeded. However, C_p^* will generally be decreased since the effect of increasing the flow through the rotor is offset by the effect of an increase in the projected area swept by the outer diameter of the flange. The present results show that the peak C_p^* of a properly designed ducted turbine can approach the BJL. For practical considerations, apart from increasing power output, the installation of a duct with inlet screens can help in the protection of marine life, and the protection of the rotor.

In the present study, the rotor is simulated by an actuator disc and the power extraction is the upper bound value corresponding to an ideal rotor with an infinite number of blades. This assumption may not be accurate if the turbines are close together as interaction among turbines may exist due to the swirling motion of blades. Therefore, in the simulation, the blockage ratio is limited to the low-value range of 0.035 to 0.131. In actual application, the reduction in power extraction due to the effects of blades should be accounted for. Generally, the efficiency achieved is below 70% (e.g. Shaaban & Hafiz, 2012). A detailed study can be carried out using CFD with the blades explicitly simulated or by conducting laboratory experiments. Also, the optimum extraction of power from an array of ducted turbines in a tidal channel is a topic worthwhile for further study.

Acknowledgements

This work is part of The Hong Kong Polytechnic University research funded by the University Grants Committee (UGC) and the Research Grants Council (RGC) of Hong Kong, SAR, China.

All the authors contributed to conceptualization, methodology, investigation, result analysis, and original drafting of the article; Li, C.W was also responsible for the supervision and revision of the article.

Disclosure statement

No potential conflict of interest was reported by the author(s).

Funding

The Hong Kong Polytechnic University International Postgraduate Scholarship funded by the University Grants Committee (UGC) and the Research Grants Council (RGC) of Hong Kong, SAR, China.

ORCID

M. Maduka  <http://orcid.org/0000-0001-7865-3958>

C.W. Li  <http://orcid.org/0000-0002-8726-613X>

References

- Abe, K., Nishida, M., Sakurai, A., Ohya, Y., Kihara, H., Wada, E., & Sato, K. (2005). Experimental and numerical investigations of flow fields behind a small wind turbine with a flanged diffuser. *Journal of Wind Engineering and Industrial Aerodynamics*, 93(12), 951–970. <https://doi.org/10.1016/j.jweia.2005.09.003>
- Abe, K. I., & Ohya, Y. (2004). An investigation of flow fields around flanged diffusers using CFD. *Journal of Wind Engineering and Industrial Aerodynamics*, 92(3–4), 315–330. <https://doi.org/10.1016/j.jweia.2003.12.003>
- Belloni, C. S. (2013). *Hydrodynamics of ducted and open-centre tidal turbines* (Doctoral dissertation, University of Oxford).
- Betz, A. (1920). Das Maximum der theoretisch möglichen Ausnutzung des Windes durch Windmotoren. *Zeitschrift für das gesamte Turbinenwesen*, 20, 307–309.
- Celik, I. B., Ghia, U., Roache, P. J., & Freitas, C. J. (2008). Procedure for estimation and reporting of uncertainty due to discretization in CFD applications. *Journal of Fluids Engineering*, 130(7), 078001. <https://doi.org/10.1115/1.2960953>
- Consul, C. A., Willden, R. H. J., & McIntosh, S. C. (2013). Blockage effects on the hydrodynamic performance of a marine cross-flow turbine. *Philosophical Transactions of the Royal Society A: Mathematical, Physical and Engineering Sciences*, 371(1985), 20120299. <https://doi.org/10.1098/rsta.2012.0299>
- Edenhofer, O., Pichs-Madruga, R., Sokona, Y., Seyboth, K., Matschoss, P., Kadner, S., & Stechow, V. (2011). *IPCC special report on renewable energy sources and climate change mitigation*. Intergovernmental Panel on Climate change (IPCC). <https://doi.org/10.1017/CBO9781139151153>
- El-Zahaby, A. M., Kabeel, A. E., Elsayed, S. S., & Obiaa, M. F. (2017). CFD analysis of flow fields for shrouded wind turbine's diffuser model with different flange angles. *Alexandria Engineering Journal*, 56(1), 171–179. <https://doi.org/10.1016/j.aej.2016.08.036>
- Fleming, C. F., & Willden, R. H. (2016). Analysis of bi-directional ducted tidal turbine performance. *International Journal of Marine Energy*, 16, 162–173. <https://doi.org/10.1016/j.ijome.2016.07.003>
- Garrett, C., & Cummins, P. (2007). The efficiency of a turbine in a tidal channel. *Journal of Fluid Mechanics*, 588, 243. <https://doi.org/10.1017/S0022112007007781>
- Geuzaine, C., & Remacle, J. F. (2009). Gmsh: A three-dimensional finite element mesh generator with built-in pre- and post-processing facilities. *International Journal for Numerical Methods in Engineering*, 79(11), 1309–1331. <https://doi.org/10.1002/nme.2579>
- Gilbert, B. L., & Foreman, K. M. (1979). Experimental demonstration of the diffuser-augmented wind turbine concept. *Journal of Energy*, 3(4), 235–240. <https://doi.org/10.2514/3.48002>
- Gilbert, B. L., Oman, R. A., & Foreman, K. M. (1978). Fluid dynamics of diffuser-augmented wind turbines. *Journal of Energy*, 2(6), 368–374. <https://doi.org/10.2514/3.47988>
- Greenshields, C. J., & Openfoam, R. (2016). *User Guide version 4.0*. OpenFOAM Foundation Ltd.
- Hansen, M. O. L., Sørensen, N. N., & Flay, R. G. J. (2000). Effect of placing a diffuser around a wind turbine. *Wind Energy*, 3(4), 207–213. <https://doi.org/10.1002/we.37>
- Houlsby, G. T., Draper, S., & Oldfield, M. L. G. (2008). Application of linear momentum actuator disc theory to open channel flow.
- Igra, O. (1976). Shrouds for aerogenerators. *AIAA Journal*, 14(10), 1481–1483. <https://doi.org/10.2514/3.61486>
- Igra, O. (1981). Research and development for shrouded wind turbines. *Energy Conversion and Management*, 21(1), 13–48. [https://doi.org/10.1016/0196-8904\(81\)90005-4](https://doi.org/10.1016/0196-8904(81)90005-4)
- Kardous, M., Chaker, R., Aloui, F., & Nasrallah, S. B. (2013). On the dependence of an empty flanged diffuser performance on flange height: Numerical simulations and PIV visualizations. *Renewable Energy*, 56, 123–128. <https://doi.org/10.1016/j.renene.2012.09.061>
- Kolekar, N., & Banerjee, A. (2015). Performance characterization and placement of a marine hydrokinetic turbine in a tidal channel under boundary proximity and blockage effects. *Applied Energy*, 148, 121–133. <https://doi.org/10.1016/j.apenergy.2015.03.052>
- Lawn, C. J. (2003). Optimization of the power output from ducted turbines. *Proceedings of the Institution of Mechanical Engineers, Part A: Journal of Power and Energy*, 217(1), 107–117. <https://doi.org/10.1243/095765003321148754>
- Lilley, G. M., & Rainbird, W. J. (1956). A preliminary report on the design and performance of ducted windmills.
- Mansour, K., & Meskinkhoda, P. (2014). Computational analysis of flow fields around flanged diffusers. *Journal of Wind Engineering and Industrial Aerodynamics*, 124, 109–120. <https://doi.org/10.1016/j.jweia.2013.10.012>
- Menter, F. R., Kuntz, M., & Langtry, R. (2003). Ten years of industrial experience with the SST turbulence model. *Turbulence, Heat and Mass Transfer*, 4(1), 625–632.
- Nieto, F., Hargreaves, D. M., Owen, J. S., & Hernández, S. (2015). On the applicability of 2D URANS and SST $k-\omega$ turbulence model to the fluid-structure interaction of rectangular cylinders. *Engineering Applications of Computational Fluid Mechanics*, 9(1), 157–173. <https://doi.org/10.1080/19942060.2015.1004817>
- Nishino, T., & Willden, R. H. (2012a). The efficiency of an array of tidal turbines partially blocking a wide channel. *Journal of Fluid Mechanics*, 708, 596–606. <https://doi.org/10.1017/jfm.2012.349>
- Nishino, T., & Willden, R. H. (2012b). Effects of 3-D channel blockage and turbulent wake mixing on the limit of power extraction by tidal turbines. *International Journal of Heat and Fluid Flow*, 37, 123–135. <https://doi.org/10.1016/j.ijheatfluidflow.2012.05.002>
- Ohya, Y., Karasudani, T., Sakurai, A., Abe, K. I., & Inoue, M. (2008). Development of a shrouded wind turbine with

- a flanged diffuser. *Journal of Wind Engineering and Industrial Aerodynamics*, 96(5), 524–539. <https://doi.org/10.1016/j.jweia.2008.01.006>
- Okulov, V. L., & Van Kuik, G. A. (2012). The Betz–Joukowski limit: On the contribution to rotor aerodynamics by the British, German, and Russian scientific schools. *Wind Energy*, 15(2), 335–344. <https://doi.org/10.1002/we.464>
- Phillips, D. G., Flay, R. G. J., & Nash, T. A. (1999). Aerodynamic analysis and monitoring of the Vortec 7 diffuser-augmented wind turbine. *Transactions of the Institution of Professional Engineers New Zealand: Electrical/Mechanical/Chemical Engineering Section*, 26(1), 13–19.
- Rahman, A., Venugopal, V., & Thiebot, J. (2018). On the accuracy of three-dimensional actuator disc approach in modelling a large-scale tidal turbine in a simple channel. *Energies*, 11(8), 2151. <https://doi.org/10.3390/en11082151>
- REN21, R. (2018). *Global Status Report, REN21 Secretariat*. Tech. Rep.
- Ross, H., & Polagye, B. (2020). An experimental assessment of analytical blockage corrections for turbines. *Renewable Energy*, 152, 1328–1341. <https://doi.org/10.1016/j.renene.2020.01.135>
- Setoguchi, T., Shiomi, N., & Kaneko, K. (2004). Development of two-way diffuser for fluid energy conversion system. *Renewable Energy*, 29(10), 1757–1771. <https://doi.org/10.1016/j.renene.2004.02.007>
- Shaaban, S., & Hafiz, A. A. (2012). Effect of duct geometry on Wells turbine performance. *Energy Conversion and Management*, 61, 51–58. <https://doi.org/10.1016/j.enconman.2012.03.023>
- Shives, M. R. (2011). *Hydrodynamic modeling, optimization and performance assessment for ducted and non-ducted tidal turbines* (Doctoral dissertation). <http://hdl.handle.net/1828/3801>.
- Shives, M., & Crawford, C. (2010, September). Overall efficiency of ducted tidal current turbines. In *OCEANS 2010 MTS/IEEE SEATTLE* (pp. 1–6). IEEE. <https://doi.org/10.1109/OCEANS.2010.5664426>.
- Shives, M., & Crawford, C. (2011). Developing an empirical model for ducted tidal turbine performance using numerical simulation results. *Proceedings of the Institution of Mechanical Engineers, Part A: Journal of Power and Energy*, 226(1), 112–125. <https://doi.org/10.1177/0957650911417958>
- Stringer, R. M., Zang, J., & Hillis, A. J. (2014). Unsteady RANS computations of flow around a circular cylinder for a wide range of Reynolds numbers. *Ocean Engineering*, 87, 1–9. <https://doi.org/10.1016/j.oceaneng.2014.04.017>
- Sun, D., Owen, J. S., & Wright, N. G. (2009). Application of the $k-\omega$ turbulence model for a wind-induced vibration study of 2D bluff bodies. *Journal of Wind Engineering and Industrial Aerodynamics*, 97(2), 77–87. <https://doi.org/10.1016/j.jweia.2008.08.002>
- Van Bussel, G. J. (2007). The science of making more torque from wind: Diffuser experiments and theory revisited. *Journal of Physics: Conference Series*, 75(1), 012010. IOP. <https://doi.org/10.1088/1742-6596/75/1/012010>
- Whelan, J. I., Graham, J. M. R., & Peiró, J. (2009). A free-surface and blockage correction for tidal turbines. *Journal of Fluid Mechanics*, 624, 281. <https://doi.org/10.1017/S002211200900591>